

Measurement of branching fractions of $\Lambda_c^+ \rightarrow pK_S^0 K_S^0$ and $\Lambda_c^+ \rightarrow pK_S^0 \eta$ at Belle

(The Belle Collaboration)

We present a study of a singly Cabibbo-suppressed decay $\Lambda_c^+ \rightarrow pK_S^0 K_S^0$ and a Cabibbo-favored decay $\Lambda_c^+ \rightarrow pK_S^0 \eta$ based on 980 fb⁻¹ of data collected by the Belle detector, operating at the KEKB energy-asymmetric e^+e^- collider. We measure their branching fractions relative to $\Lambda_c^+ \rightarrow pK_S^0$: $\mathcal{B}(\Lambda_c^+ \rightarrow pK_S^0 K_S^0)/\mathcal{B}(\Lambda_c^+ \rightarrow pK_S^0) = (1.47 \pm 0.08 \pm 0.04) \times 10^{-2}$ and $\mathcal{B}(\Lambda_c^+ \rightarrow pK_S^0 \eta)/\mathcal{B}(\Lambda_c^+ \rightarrow pK_S^0) = (2.72 \pm 0.06 \pm 0.13) \times 10^{-1}$. Combining with the world average $\mathcal{B}(\Lambda_c^+ \rightarrow pK_S^0)$, we have the absolute branching fractions, $\mathcal{B}(\Lambda_c^+ \rightarrow pK_S^0 K_S^0) = (2.34 \pm 0.12 \pm 0.06 \pm 0.12) \times 10^{-4}$ and $\mathcal{B}(\Lambda_c^+ \rightarrow pK_S^0 \eta) = (4.32 \pm 0.10 \pm 0.20 \pm 0.22) \times 10^{-3}$. The first and second uncertainties are statistical and systematic, respectively, while the third ones arise from the uncertainty on $\mathcal{B}(\Lambda_c^+ \rightarrow pK_S^0)$. The $\Lambda_c^+ \rightarrow pK_S^0 K_S^0$ is observed for the first time and has a statistical significance more than 10σ , and the branching fraction of $\Lambda_c^+ \rightarrow pK_S^0 \eta$ is consistent with the world average but has a threefold improvement of precision.

I. INTRODUCTION

The weak decays of charmed baryons provide an excellent platform for understanding Quantum Chromodynamics with transitions involving the charm quark. Their decay amplitudes consist of factorizable and non-factorizable contributions. The latter may play a non-trivial or essential role in the decay amplitude and are described by various approaches, including the pole model [1, 2], the covariant confined quark model [3, 4], current algebra [5–7] and SU(3)_F symmetry [8–10]. To date, there is no established phenomenological model to describe the complicated physics of baryon decays. Precise measurements of branching fractions of charmed baryon weak decays are useful to study the dynamics of charmed baryons and test the predictions of theoretical models. In addition, the singly Cabibbo-suppressed (SCS) charm decays are essential probes to search for CP violation in the charm sector [11–13] and hunt for new physics beyond the standard model [14–16].

Experimentally, the investigation of weak decays of charmed baryons is more challenging than that of charmed mesons, mainly due to lower production rates. For the lightest state, Λ_c^+ , hadronic modes have been studied at several experiments, but some of them have yet to be observed or the precision can be much improved [17]. The Cabibbo-favored (CF) $\Lambda_c^+ \rightarrow pK_S^0 \eta$ and the SCS $\Lambda_c^+ \rightarrow pK_S^0 K_S^0$ decays are two examples [18]. For $\Lambda_c^+ \rightarrow pK_S^0 \eta$, the world average branching fraction, $\mathcal{B}(\Lambda_c^+ \rightarrow pK_S^0 \eta) = (4.15 \pm 0.90) \times 10^{-3}$ [17], still has a large uncertainty (22%). The $\Lambda_c^+ \rightarrow pK_S^0 K_S^0$, of which the predicted branching fraction is $\mathcal{B}(\Lambda_c^+ \rightarrow pK_S^0 K_S^0) = (1.9 \pm 0.4) \times 10^{-3}$ based on SU(3)_F symmetry [19], has not previously been observed.

In this paper, we present a precise measurement of $\mathcal{B}(\Lambda_c^+ \rightarrow pK_S^0 K_S^0)$ and $\mathcal{B}(\Lambda_c^+ \rightarrow pK_S^0 \eta)$ based on the full Belle dataset. These three-body decay modes also allow the study of intermediate states, such as the $N^*(1535)$, the nature of which is still unknown. Understanding the nature of $N^*(1535)$ is very challenging and important in hadron physics. The $N^*(1535)$, with spin parity

$J^P = 1/2^-$, has a larger mass than the radial excitation $N^*(1440)$, which is opposite to the prediction in classical constituent quark models [20]. It also couples strongly to channels with strangeness, such as ηN and $K\Lambda$, which is difficult to explain within the naive constituent quark models [21, 22]. The inclusion of five-quark components gives a natural explanation for these properties [23]. The $\Lambda_c^+ \rightarrow pK_S^0 \eta$ decay, in which the final-state $p\eta$ is in a pure isospin $I = 1/2$ state, is an ideal process to study the $N^*(1535)$ resonance, since $N^*(1535)$ has a large branching ratio to $p\eta$, in S -wave. The other interesting intermediate resonances are $a_0(980)$ and $f_0(980)$ in $\Lambda_c^+ \rightarrow pK_S^0 K_S^0$ since they both couple to $K\bar{K}$. The nature of the light scalars $f_0(980)$ and $a_0(980)$ remains not fully understood and continues to cause controversy [24–26], but they are often interpreted as compact tetraquark states [27–29] or $K\bar{K}$ bound states [30, 31]. Therefore, we reconstruct the Dalitz plots of $\Lambda_c^+ \rightarrow pK_S^0 K_S^0$ and $\Lambda_c^+ \rightarrow pK_S^0 \eta$ decays to check such interesting intermediate resonances.

II. DETECTOR AND DATA SET

This analysis uses the full dataset recorded by the Belle detector [32] operating at the KEKB energy-asymmetric e^+e^- collider [33]. This data sample corresponds to a total integrated luminosity of 980 fb⁻¹ collected at or near the $\Upsilon(nS)$ ($n = 1, 2, 3, 4, 5$) resonances. The Belle detector is a large-solid-angle magnetic spectrometer consisting of a silicon vertex detector, a central drift chamber (CDC), an array of aerogel threshold Cherenkov counters (ACC), a barrel-like arrangement of time-of-flight scintillation counters (TOF), and an electromagnetic calorimeter (ECL) consisting of CsI(Tl) crystals. These components are all located inside a superconducting solenoid coil that provides a 1.5 T magnetic field. The iron flux-return of the magnet is instrumented to detect K_L^0 mesons and to identify muons. The detector is described in detail elsewhere [32].

Monte Carlo (MC) simulated events are generated with EVTGEN [34] and PYTHIA [35], and are subsequently pro-

cessed through the full detector simulation based on GEANT3 [36]. Final-state radiation from charged particles is included at the event generation stage using PHOTOS [37]. “Generic” MC samples include $B\bar{B}$ events and continuum processes $e^+e^- \rightarrow q\bar{q}$ ($q = u, d, s, c$) corresponding to an integrated luminosity three times that of the data. Samples of MC events of Λ_c^+ signal decay modes are produced in the $e^+e^- \rightarrow c\bar{c}$ process, decayed uniformly in three-body phase space, and used to study the efficiency.

III. EVENT SELECTION

We reconstruct the two signal modes $\Lambda_c^+ \rightarrow pK_S^0K_S^0$ and $\Lambda_c^+ \rightarrow pK_S^0\eta$ and their reference mode $\Lambda_c^+ \rightarrow pK_S^0$. The event selections are optimized based on a figure of merit (FOM), defined as $\text{FOM} = N_S/\sqrt{N_B}$ for $\Lambda_c^+ \rightarrow pK_S^0K_S^0$ due to its branching fraction having not yet been measured, and $\text{FOM} = N_S/\sqrt{N_S + N_B}$ for $\Lambda_c^+ \rightarrow pK_S^0\eta$ assuming its current world average branching fraction [17]. Here N_S and N_B are the expected yields of signal and background, respectively, based on numbers of candidates in the $M(\Lambda_c^+)$ signal regions, where $M(\Lambda_c^+)$ is the invariant mass of reconstructed Λ_c^+ candidates. These signal regions are defined to be within 10, 22, and 18 MeV/c^2 of the nominal Λ_c^+ mass [17] for the $\Lambda_c^+ \rightarrow pK_S^0K_S^0$, $\Lambda_c^+ \rightarrow pK_S^0\eta$, and $\Lambda_c^+ \rightarrow pK_S^0$ channels, respectively; each signal band includes $\approx 98\%$ of the signal. For the expected background, N_B , the number found in MC is multiplied by the data/MC yield ratio in the $M(\Lambda_c^+)$ sideband region ($30 < |M(\Lambda_c^+) - m_{\Lambda_c^+}| < 50 \text{ MeV}/c^2$), where $m_{\Lambda_c^+}$ is the nominal Λ_c^+ mass [17].

The particle identification (PID) likelihood for a given particle hypothesis, \mathcal{L}_i ($i = \pi, K, p$), is calculated from the photon yield in the ACC, energy-loss measurements in the CDC, and time-of-flight information from the TOF [38]. Charged tracks satisfying $\mathcal{R}(p|K) = \mathcal{L}_p/(\mathcal{L}_p + \mathcal{L}_K) > 0.6$ and $\mathcal{R}(p|\pi) = \mathcal{L}_p/(\mathcal{L}_p + \mathcal{L}_\pi) > 0.6$, are identified as protons. These PID requirements have signal efficiencies of 94% for $\Lambda_c^+ \rightarrow pK_S^0K_S^0$ and 97% for $\Lambda_c^+ \rightarrow pK_S^0\eta$.

For proton candidates, the point on the track nearest to the axis defined by the positron beam and in the direction opposite to it (“ z -axis”) is required to be within 3.0 cm of the interaction point in the z -direction and within 1.0 cm on the transverse (x - y) plane. This requirement rejects tracks not originating at the interaction point (IP) and introduces a negligible signal efficiency loss ($< 0.01\%$).

Candidate K_S^0 ’s are reconstructed from pairs of oppositely-charged tracks, treated as pions, using an artificial neural network (NN) [39]. The NN utilizes the following 13 input variables: the K_S^0 momentum in the laboratory frame; the separation in z between the two π^\pm tracks at their intersection in the x - y plane; for each track, the nearest distance to the IP in the x - y plane; the

K_S^0 flight length in the x - y plane; the angle between the K_S^0 momentum and the vector joining the IP to the K_S^0 decay vertex; in the K_S^0 rest frame, the angle between the π^+ momentum and the laboratory-frame boost direction; and, for each π^\pm track, the number of CDC hits in both stereo and axial views, and the presence or absence of SVD hits. Detailed information is provided elsewhere [40]. The invariant mass of the reconstructed $K_S^0 \rightarrow \pi^+\pi^-$ candidate is required to lie within $10 \text{ MeV}/c^2$ of the nominal K_S^0 mass [17]; this includes 99.9% of the K_S^0 signal. The two pion tracks from each K_S^0 candidate are refitted to originate from a common vertex and constrained to have invariant mass equal to the nominal K_S^0 mass [17]. The corresponding fit quality $\chi_{\text{mv}}^2(K_S^0)$ is required to be smaller than 100. The selected K_S^0 sample has a purity of greater than 98%.

Photon candidates are identified as energy clusters in the ECL that are not associated with any charged track. The ratio of the energy deposited in the 3×3 array of crystals centered on the crystal with the highest energy, to the energy deposited in the corresponding 5×5 array of crystals, is required to be greater than 0.8. The photon energy is required to be greater than 50 MeV in the barrel region (covering the polar angle $32^\circ < \theta < 129^\circ$), and greater than 100 MeV in the endcap region ($12^\circ < \theta < 31^\circ$ or $132^\circ < \theta < 157^\circ$).

Candidate $\eta \rightarrow \gamma\gamma$ decays are reconstructed from photon pairs having an invariant mass satisfying $500 \text{ MeV}/c^2 < M(\gamma\gamma) < 580 \text{ MeV}/c^2$ (3σ in $M_\eta(\gamma\gamma)$ resolution). The invariant mass of each η candidate is constrained to the nominal η mass [17] at the Λ_c^+ decay vertex (described below). The fit quality of this mass constraint is required to satisfy $\chi_m^2(\eta) < 8$, and the resulting η momentum in the laboratory frame is required to be greater than $0.4 \text{ GeV}/c$. To further suppress the background, η candidates are vetoed if either of daughters can be paired with another photon such that the $\gamma\gamma$ pair has an invariant mass within 2.5σ of the nominal π^0 mass ($\sigma = 5 \text{ MeV}/c^2$). This π^0 -veto results in a signal loss of 28% and removes 72% of background.

The Λ_c^+ candidates are assembled by forming combinations of the final-state particles for each mode. The p and K_S^0 are required to originate from a common vertex (denoted the Λ_c^+ decay vertex and the K_S^0 production vertex) with a fit quality $\chi_{\text{vtx}}^2 < 24$. To reduce combinatorial background, the scaled momentum of the Λ_c^+ candidate, defined as $x_p = p^*c/\sqrt{s/4 - M^2(\Lambda_c^+) \cdot c^4}$, is required to be greater than 0.48, where s is the square of the center-of-mass energy and p^* is the momentum of reconstructed Λ_c^+ candidates in the e^+e^- center-of-mass frame.

For the SCS decay $\Lambda_c^+ \rightarrow pK_S^0K_S^0$, a non- K_S^0 peaking background from the CF decay $\Lambda_c^+ \rightarrow pK_S^0\pi^+\pi^-$ exists, even though it is suppressed by the vertex fit and K_S^0 selection. The K_S^0 decay length L is determined by the

projection of the vector joining the K_S^0 production and decay vertices onto the K_S^0 momentum direction, and its corresponding uncertainty σ_L is calculated by propagating uncertainties in the vertices and the K_S^0 momentum, including their correlations. To suppress the non- K_S^0 peaking CF background, we require the significance of the K_S^0 decay length $L/\sigma_L(K_S^0) > 10$ for the slower of the two K_S^0 's in $\Lambda_c^+ \rightarrow pK_S^0K_S^0$. This requirement reduces the signal efficiency by 3%, and rejects 80% of non- K_S^0 peaking background. The remaining non- K_S^0 peaking background is ignored in the $M(\Lambda_c^+)$ fits because it has a tiny ratio 0.4% to signal based on the MC studies with the branching fraction $(1.6 \pm 0.12)\%$ [17], but considered in the systematic uncertainty.

After applying all selection criteria to the data, we find 1.03, 1.06, and 1.01 candidates per event for $\Lambda_c^+ \rightarrow pK_S^0K_S^0$, $\Lambda_c^+ \rightarrow pK_S^0\eta$, and $\Lambda_c^+ \rightarrow pK_S^0$, respectively, in candidates selected from the entire $M(\Lambda_c^+)$ fit region ($|M(\Lambda_c^+) - m_{\Lambda_c^+}| < 0.05 \text{ GeV}/c^2$). Correspondingly, about 3.1%, 5.7% and 1.2% of events have multiple signal candidates, which do not introduce any peaking background. We retain all candidates for this branching fraction measurement.

IV. YIELD EXTRACTION

The signal yield is extracted by an unbinned extended maximum likelihood fit to the $M(\Lambda_c^+)$ distribution. The signal probability density function (PDF) is a sum of three symmetric Gaussian functions for the $\Lambda_c^+ \rightarrow pK_S^0K_S^0$ mode, a sum of one symmetric Gaussian and two asymmetric Gaussians for the $\Lambda_c^+ \rightarrow pK_S^0\eta$ mode, and a sum of one symmetric Gaussian and three asymmetric Gaussians for the $\Lambda_c^+ \rightarrow pK_S^0$ mode. The Gaussian functions share a common mean parameter but have different width parameters. The fit is first performed on truth-matched signal MC events.

In fitting data, the mean is allowed a common shift (δ_μ) from the value found in MC, and the widths are those found in MC, multiplied by a common scaling factor (k_σ). The background PDF is a first-order polynomial function for $\Lambda_c^+ \rightarrow pK_S^0K_S^0$ and a second-order polynomial function for $\Lambda_c^+ \rightarrow pK_S^0\eta$ and $\Lambda_c^+ \rightarrow pK_S^0$. The background parameters are floated to account for differences between the experimental data and MC simulated samples. The results are shown in Fig. 1, along with the pulls $(N_{\text{data}} - N_{\text{fit}})/\sigma_{\text{data}}$ where σ_{data} is the error on N_{data} . The pull distributions demonstrate that the data are statistically consistent with the fitted shapes. The signal and background yields are listed in Table I.

For the $\Lambda_c^+ \rightarrow pK_S^0K_S^0$ mode, we obtain the difference in the log likelihoods obtained from fits performed with and without a signal PDF, $\Delta \ln \mathcal{L} = 524$; as the number of degrees of freedom without a signal component is three less than that with a signal component (parameters N_{sig} ,

δ_μ and k_σ are dropped), and this value of $\Delta \ln \mathcal{L}$ corresponds to a statistical significance greater than 10σ . This measurement constitutes the first observation of this SCS Λ_c^+ decay.

TABLE I. The fitted yields of signal and background in the overall fit region (FR) and the signal region (SR) for the $\Lambda_c^+ \rightarrow pK_S^0K_S^0$, $\Lambda_c^+ \rightarrow pK_S^0\eta$, and $\Lambda_c^+ \rightarrow pK_S^0$ modes. For the definition of these regions, see the text.

Yields	$\Lambda_c^+ \rightarrow pK_S^0K_S^0$	$\Lambda_c^+ \rightarrow pK_S^0\eta$	$\Lambda_c^+ \rightarrow pK_S^0$
$N_{\text{sig}}^{\text{FR}}$	2442 ± 103	12877 ± 317	515296 ± 1129
$N_{\text{bkg}}^{\text{FR}}$	41138 ± 222	75144 ± 403	627427 ± 1177
$N_{\text{sig}}^{\text{SR}}$	2391 ± 101	12641 ± 311	500457 ± 1096
$N_{\text{bkg}}^{\text{SR}}$	8228 ± 44	32935 ± 177	226055 ± 424

V. BRANCHING FRACTION

For the three-body decay modes, the Dalitz plots for candidates in the $M(\Lambda_c^+)$ signal region and sideband region are shown in Figs. 2(a, b) for $\Lambda_c^+ \rightarrow pK_S^0K_S^0$ and Figs. 2(d, e) for $\Lambda_c^+ \rightarrow pK_S^0\eta$. For $\Lambda_c^+ \rightarrow pK_S^0K_S^0$, Bose symmetry requires invariance under the exchange of the two K_S^0 's, hence the Dalitz plot for two pK_S^0 masses is symmetric. We plot $M^2(pK_S^0)_{\text{max}}$ versus $M^2(pK_S^0)_{\text{min}}$ in half of the Dalitz plot, as shown in Figs. 2(a-c), and use it to measure the branching fraction.

For each mode, a large MC sample of signal events, generated uniformly across the decay phase space, is used to determine the reconstruction efficiency. For $\Lambda_c^+ \rightarrow pK_S^0K_S^0$ and $\Lambda_c^+ \rightarrow pK_S^0\eta$, the efficiencies are calculated in bins across the phase space, based on truth-matched signal yield in the $M(\Lambda_c^+)$ signal region. The results are shown in Fig. 2(c) for $\Lambda_c^+ \rightarrow pK_S^0K_S^0$ and Fig. 2(f) for $\Lambda_c^+ \rightarrow pK_S^0\eta$. For the reference mode $\Lambda_c^+ \rightarrow pK_S^0$, the efficiency is $\varepsilon_0 = (33.85 \pm 0.05)\%$ in the $M(\Lambda_c^+)$ fit region.

For $\Lambda_c^+ \rightarrow pK_S^0K_S^0$ and $\Lambda_c^+ \rightarrow pK_S^0\eta$, we correct for efficiency bin-by-bin across the phase space. The Dalitz plots are divided uniformly into 7×7 bins for $\Lambda_c^+ \rightarrow pK_S^0K_S^0$ and 5×5 bins for $\Lambda_c^+ \rightarrow pK_S^0\eta$, as shown in Figs. 2(c, f) respectively. The efficiency-corrected yields are

$$N_{\text{corr}} = \sum_i (N_i^{\text{tot}} - N_{\text{bkg}}^{\text{SR}} f_i^{\text{bkg}}) / \varepsilon_i, \quad (1)$$

where N_i^{tot} is the raw yield in the i^{th} bin of the Dalitz plot in $M(\Lambda_c^+)$ signal region, $N_{\text{bkg}}^{\text{SR}}$ is the fitted background yield as listed in Table I, f_i^{bkg} is the fraction of background in the i^{th} -bin, with $\sum_i f_i = 1$. These fractions are obtained from the Dalitz plot distribution of events in the $M(\Lambda_c^+)$ sideband region, shown in Fig. 2(b) for $\Lambda_c^+ \rightarrow pK_S^0K_S^0$ and Fig. 2(e) for $\Lambda_c^+ \rightarrow pK_S^0\eta$. Using

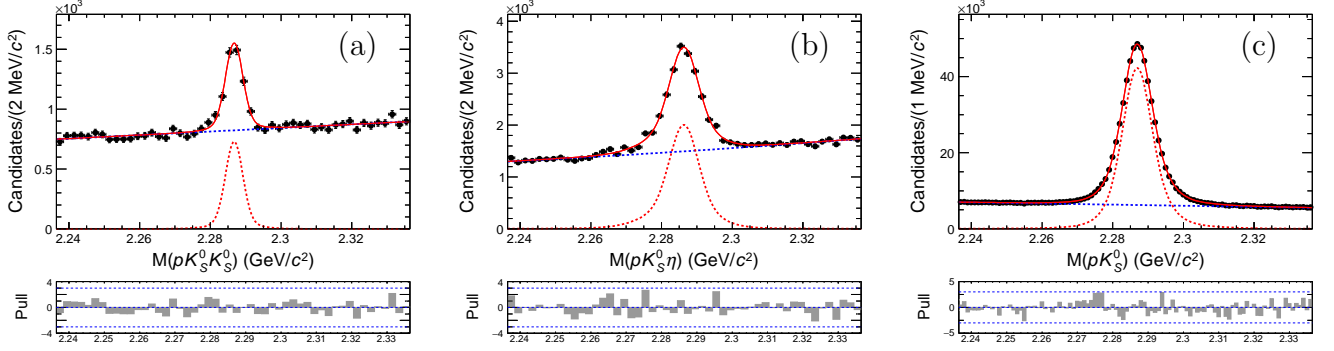


FIG. 1. The distributions of invariant mass of Λ_c^+ candidates (points with error bars) and corresponding fit results (red curves) for (a) $\Lambda_c^+ \rightarrow p K_S^0 K_S^0$, (b) $\Lambda_c^+ \rightarrow p K_S^0 \eta$, and (c) $\Lambda_c^+ \rightarrow p K_S^0$, respectively. The red (blue) dashed histograms show the signal (background).

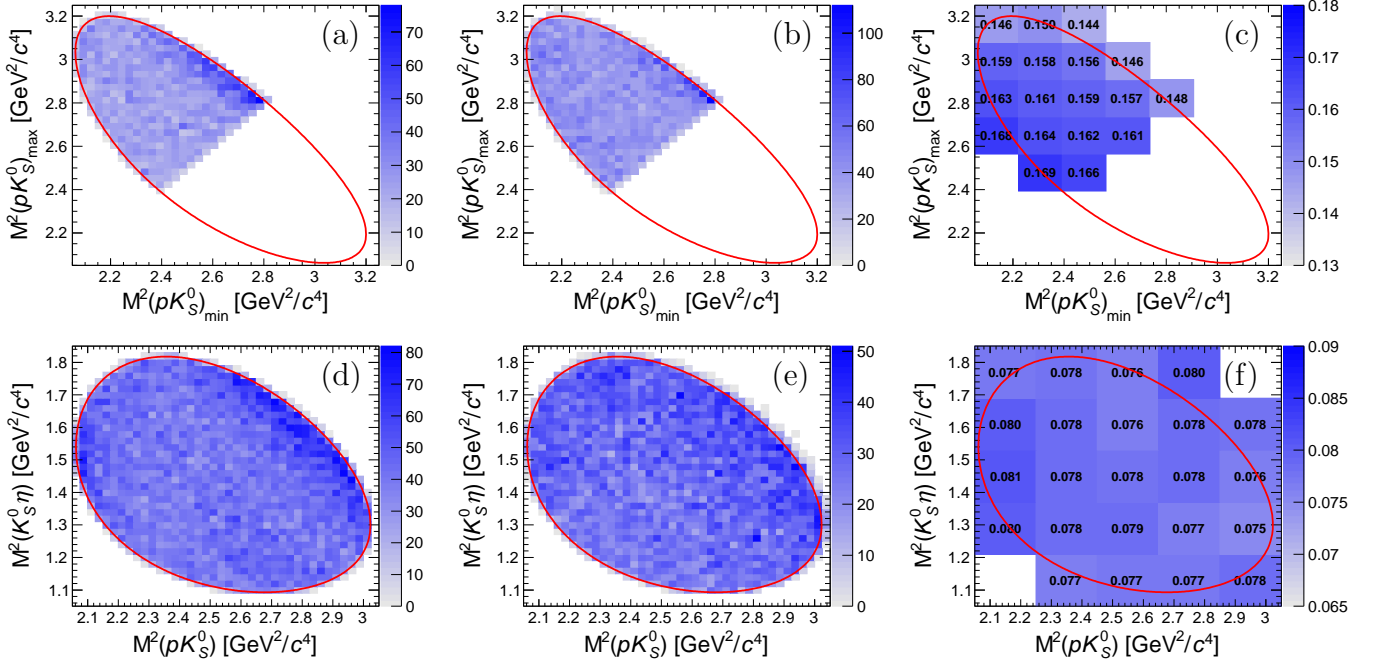


FIG. 2. Plots (a, d) show the Dalitz plots in the $M(\Lambda_c^+)$ signal region, and (b, e) show the Dalitz plots in the $M(\Lambda_c^+)$ sideband region for $\Lambda_c^+ \rightarrow p K_S^0 K_S^0$ (top) and $\Lambda_c^+ \rightarrow p K_S^0 \eta$ (bottom). Plots (c, f) show the average signal efficiency in bins across the Dalitz plane. The red curves show the edges of kinematic phase-space region of the decays.

the generic MC sample, we find that the Dalitz plot in the chosen $M(\Lambda_c^+)$ sideband region is consistent with the generic background in the $M(\Lambda_c^+)$ signal region. The uncertainties on each variable in Eq. (1) have been considered and are propagated into the efficiency-corrected yields, N_{corr} . We obtain

$$N_{\text{corr}}(\Lambda_c^+ \rightarrow p K_S^0 K_S^0) = (1.55 \pm 0.08) \times 10^4, \quad (2)$$

$$N_{\text{corr}}(\Lambda_c^+ \rightarrow p K_S^0 \eta) = (1.63 \pm 0.04) \times 10^5. \quad (3)$$

erence mode are determined by Eqs. (4, 5).

$$\frac{\mathcal{B}(\Lambda_c^+ \rightarrow p K_S^0 K_S^0)}{\mathcal{B}(\Lambda_c^+ \rightarrow p K_S^0)} = \frac{N_{\text{corr}}(\Lambda_c^+ \rightarrow p K_S^0 K_S^0)}{\mathcal{B}(K_S^0 \rightarrow \pi^+ \pi^-) N_{\text{sig}}^{\text{FR}}(\Lambda_c^+ \rightarrow p K_S^0) / \varepsilon_0}, \quad (4)$$

$$\frac{\mathcal{B}(\Lambda_c^+ \rightarrow p K_S^0 \eta)}{\mathcal{B}(\Lambda_c^+ \rightarrow p K_S^0)} = \frac{N_{\text{corr}}(\Lambda_c^+ \rightarrow p K_S^0 \eta)}{\mathcal{B}(\eta \rightarrow \gamma \gamma) N_{\text{sig}}^{\text{FR}}(\Lambda_c^+ \rightarrow p K_S^0) / \varepsilon_0}. \quad (5)$$

Inserting the efficiency-corrected yields in Eqs. (2, 3), $N_{\text{sig}}^{\text{FR}}(\Lambda_c^+ \rightarrow p K_S^0)$ in Table I and ε_0 for $\Lambda_c^+ \rightarrow p K_S^0$, and the world averages $\mathcal{B}(K_S^0 \rightarrow \pi^+ \pi^-) = (69.20 \pm 0.05)\%$ and

The relative branching fractions of signal modes to ref-

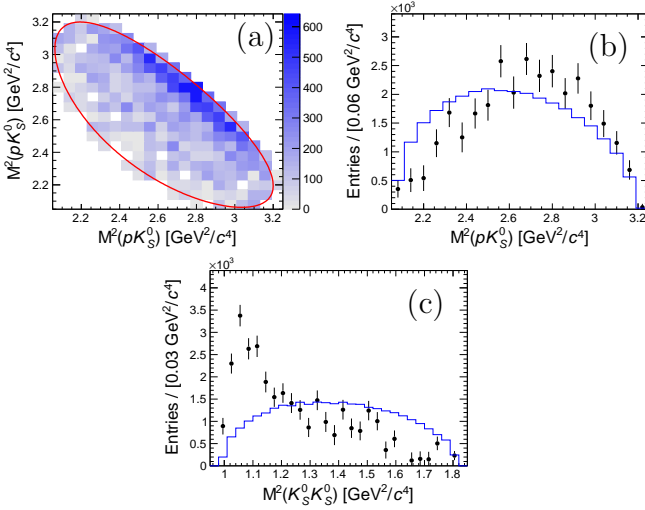


FIG. 3. For $\Lambda_c^+ \rightarrow p K_S^0 K_S^0$, the Dalitz plot after background subtraction and efficiency correction bin-by-bin and its projections superimposing with signal MC produced by phase space mode (blue histograms). This symmetric Dalitz plot and its projections show two entries per candidate, one for each possible $p K_S^0$ combination. A dominant structure near the $K_S^0 K_S^0$ threshold, which we identify with $f_0(980)$ or $a_0(980)^0$, is clearly seen.

$\mathcal{B}(\eta \rightarrow \gamma\gamma) = (39.41 \pm 0.20)\%$ [17], we find

$$\frac{\mathcal{B}(\Lambda_c^+ \rightarrow p K_S^0 K_S^0)}{\mathcal{B}(\Lambda_c^+ \rightarrow p K_S^0 \eta)} = (1.47 \pm 0.08) \times 10^{-2}, \quad (6)$$

$$\frac{\mathcal{B}(\Lambda_c^+ \rightarrow p K_S^0 \eta)}{\mathcal{B}(\Lambda_c^+ \rightarrow p K_S^0)} = (2.72 \pm 0.06) \times 10^{-1}, \quad (7)$$

Combining with the world average branching fraction of reference mode $\mathcal{B}(\Lambda_c^+ \rightarrow p K_S^0) = (1.59 \pm 0.08)\%$ [17], we have the absolute branching fractions:

$$\mathcal{B}(\Lambda_c^+ \rightarrow p K_S^0 K_S^0) = (2.34 \pm 0.12 \pm 0.12) \times 10^{-4}, \quad (8)$$

$$\mathcal{B}(\Lambda_c^+ \rightarrow p K_S^0 \eta) = (4.32 \pm 0.10 \pm 0.22) \times 10^{-3}, \quad (9)$$

where the uncertainties are statistical and from the uncertainty on $\mathcal{B}(\Lambda_c^+ \rightarrow p K_S^0)$.

We examine the Dalitz plots for $\Lambda_c^+ \rightarrow p K_S^0 K_S^0$ and $\Lambda_c^+ \rightarrow p K_S^0 \eta$, after background subtraction and efficiency correction, for intermediate resonances. In $\Lambda_c^+ \rightarrow p K_S^0 K_S^0$, clear evidence for $f_0(980)$ or $a_0(980)^0$ (labeled as $S_0(980)$) near the $K_S^0 K_S^0$ threshold is seen, as shown in Fig. 3. In $\Lambda_c^+ \rightarrow p K_S^0 \eta$, a significant enhancement consistent with $N^*(1535)$ is found near the $p\eta$ threshold, as shown in Fig. 4. In the future, amplitude analyses of these decays can be expected to improve our understanding of the nature of $S_0(980)$ and $N^*(1535)$.

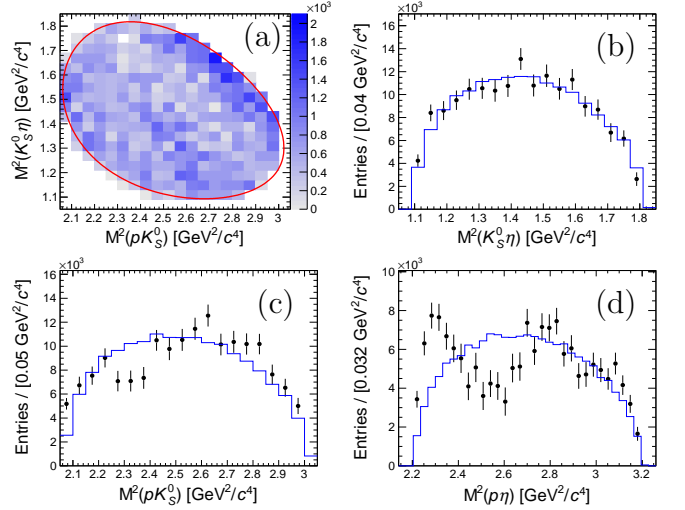


FIG. 4. For $\Lambda_c^+ \rightarrow p K_S^0 \eta$, the Dalitz plot after background subtraction and efficiency correction bin-by-bin and its projections superimposing with signal MC produced by phase space mode (blue histograms). A significant structure of $N^*(1535)$ near the $p\eta$ threshold is found.

VI. SYSTEMATIC UNCERTAINTY

In measuring the ratio of branching fractions, many systematic uncertainties cancel, as they affect both the signal and reference modes. The remaining systematic uncertainties are summarized in Table II and introduced in detail below.

TABLE II. Relative systematic uncertainties of the branching fractions of $\Lambda_c^+ \rightarrow p K_S^0 K_S^0$ and $\Lambda_c^+ \rightarrow p K_S^0 \eta$, and the uncertainty from the branching fraction of the reference mode.

sources	$\mathcal{B}_{\Lambda_c^+ \rightarrow p K_S^0 K_S^0}$	$\mathcal{B}_{\Lambda_c^+ \rightarrow p K_S^0 \eta}$
K_S^0 reconstruction	1.4%	0.4%
proton PID efficiency	0.9%	0.5%
η reconstruction	–	4.0%
$M(\Lambda_c^+)$ fit procedure	1.9%	2.3%
efficiency-correction procedure	0.6%	0.4%
non- K_S^0 peaking background	0.8%	–
$\delta\mathcal{B}/\mathcal{B}(K_S^0 \rightarrow \pi^+ \pi^-, \eta \rightarrow \gamma\gamma)$	0.1%	0.5%
total syst. uncertainty	2.7%	4.7%
$\delta\mathcal{B}/\mathcal{B}(\Lambda_c^+ \rightarrow p K_S^0)$	5.0%	5.0%

The systematic uncertainty associated with the K_S^0 reconstruction is considered as follows. A table of K_S^0 efficiency ratios of data to MC in eight bins of the K_S^0 momentum distribution, $R_\varepsilon^{K_S^0}$, is determined based on a control sample $D^{\pm\pm} \rightarrow (D^0 \rightarrow K_S^0 \pi^0) \pi^{\pm\pm}$. The unfolded momentum distribution in data of K_S^0 from signal is obtained using the $sPlot$ technique [41]. From one $R_\varepsilon^{K_S^0}$ table, we can determine the average ratios: (1) for

$\Lambda_c^+ \rightarrow pK_{S,\text{fast}}^0 K_{S,\text{slow}}^0$ where the subscript ‘fast’ (‘slow’) indicates the faster (slower) of two K_S^0 ’s in the final state, $\overline{R}_\varepsilon^{K_S^0} = \sum_i^8 \sum_j^8 N_{ij} (R_{\varepsilon,i}^{K_{S,\text{fast}}^0} R_{\varepsilon,j}^{K_{S,\text{slow}}^0}) / \sum_i^8 \sum_j^8 N_{ij}$ calculated on the two-dimensional $(p_{K_{S,\text{fast}}^0}, p_{K_{S,\text{slow}}^0})$ distribution due to the correlations between the momenta of two K_S^0 ’s. Here N_{ij} and $(R_{\varepsilon,i}^{K_{S,\text{fast}}^0}, R_{\varepsilon,j}^{K_{S,\text{slow}}^0})$ are the yield and the averaged $R_\varepsilon^{K_S^0}$, respectively, in the bin of i^{th} row and j^{th} column of such two-dimensional momenta distribution; (2) for $\Lambda_c^+ \rightarrow pK_S^0(\eta)$, $\overline{R}_\varepsilon^{K_S^0} = \sum_i^8 N_i R_{\varepsilon,i}^{K_S^0} / \sum_i^8 N_i$ calculated on the one-dimensional $p_{K_S^0}$ distribution. Here N_i and $R_{\varepsilon,i}^{K_S^0}$ are the yield and the averaged $R_\varepsilon^{K_S^0}$, respectively, in the i^{th} bin of such one-dimensional distribution. We build 10000 $R_\varepsilon^{K_S^0}$ tables by randomly fluctuating $R_{\varepsilon,i}^{K_S^0}$ in each bin according to its uncertainty and calculate $\overline{R}_\varepsilon^{K_S^0}$ for each. We take the mean and root-mean-square (RMS) values from the distribution of $\overline{R}_{\varepsilon,\text{sig.}}^{K_S^0} / \overline{R}_{\varepsilon,\text{ref.}}^{K_S^0} - 1$, where the subscripts ‘sig.’ and ‘ref.’ refer to the signal and reference modes, respectively, and add in quadrature as the estimate of the systematic uncertainty.

Since the protons in the signal and reference modes have different kinematic distributions, the systematic effects due to PID do not cancel completely. The data/MC ratio of proton PID efficiency depends on the proton momentum and polar angle: $R_\varepsilon^p(p, \cos\theta)$. Such a R_ε^p map is determined based on an inclusive sample of $\Lambda \rightarrow p\pi^-$. Following steps similar to those used above for K_S^0 efficiency, we obtain the unfolded $(p, \cos\theta)$ two-dimensional distribution for protons using the $sPlot$ technique [41], and plot the $\overline{R}_{\varepsilon,\text{sig.}}^p / \overline{R}_{\varepsilon,\text{ref.}}^p - 1$ values based on 10000 maps of $R_\varepsilon^p(p, \cos\theta)$. The systematic uncertainty due to PID is obtained by adding in quadrature the mean and RMS values of the $\overline{R}_{\varepsilon,\text{sig.}}^p / \overline{R}_{\varepsilon,\text{ref.}}^p - 1$ distribution.

The uncertainty due to $\eta \rightarrow \gamma\gamma$ reconstruction is estimated to be 4%, considering 2% per photon according to a study of radiative Bhabha events.

The systematic uncertainties from the $M(\Lambda_c^+)$ fits for $\Lambda_c^+ \rightarrow pK_S^0 K_S^0$ and $\Lambda_c^+ \rightarrow pK_S^0 \eta$ channels are evaluated to be 1.8% and 2.3%, respectively, after considering two sources below. (a) The uncertainty due to fixing the signal parameters in the fits is estimated by randomly varying them via a multiple-dimensional Gaussian function (including these parameters’ uncertainties and their correlation matrix from the $M(\Lambda_c^+)$ fit of truth-matched signals). We produce 1000 sets of such signal parameters and repeat the $M(\Lambda_c^+)$ fits. We take the ratio of RMS to mean value of the distribution of fitted yield as the relative systematic uncertainty: 0.2% for $\Lambda_c^+ \rightarrow pK_S^0 K_S^0$, 0.4% for $\Lambda_c^+ \rightarrow pK_S^0 \eta$, and 0.2% for $\Lambda_c^+ \rightarrow pK_S^0$. (b) To evaluate the potential fit bias, we perform a bias check for the fitted signal yield based on 1000 sets of MC samples, of which the signals are randomly sampled from a large signal MC sample and the backgrounds from the generic $B\overline{B}$ and continuum MC samples. Their sampled

yields are equal to the fitted yields in Table I. We perform $M(\Lambda_c^+)$ fits for these samples. The fitted signal yields are plotted and fitted with a Gaussian function. The shifts of the fitted mean values of the Gaussian functions from the corresponding input values are assigned as systematic uncertainties: 1.9% for $\Lambda_c^+ \rightarrow pK_S^0 K_S^0$, 2.3% for $\Lambda_c^+ \rightarrow pK_S^0 \eta$, and 0.1% for $\Lambda_c^+ \rightarrow pK_S^0$. The uncertainties for signal modes and reference mode are added in quadrature, as listed in Table II.

The systematic effects from the efficiency corrections for the $\Lambda_c^+ \rightarrow pK_S^0 K_S^0$ and $\Lambda_c^+ \rightarrow pK_S^0 \eta$ channels are evaluated to be 0.6% and 0.4%, respectively, which are obtained by taking the quadratic sum of the following sources: (a) Varying bin size: the 7×7 bins are changed to 6×6 and 8×8 bins for $\Lambda_c^+ \rightarrow pK_S^0 K_S^0$ and the 5×5 bins are changed to 4×4 and 6×6 bins for $\Lambda_c^+ \rightarrow pK_S^0 \eta$. The changes of efficiency-corrected yields, 0.2% for $\Lambda_c^+ \rightarrow pK_S^0 K_S^0$ and 0.1% for $\Lambda_c^+ \rightarrow pK_S^0 \eta$, are assigned as the systematic uncertainties. (b) To estimate the uncertainties due to the background Dalitz plot, we shift the $M(\Lambda_c^+)$ sideband region by ± 5 MeV, and repeat the efficiency correction. The resulting changes of efficiency-corrected yields, 0.1% for both channels, are assigned as systematic uncertainty. (c) The signal efficiency effects due to the additional requirements in the signal mode with respect to the reference mode, such as $p(\eta)$, $\chi_m^2(\eta)$, and $L/\sigma_L(K_S^0)$, are neglected, as the signal distributions unfolded from data using the $sPlot$ technique [41] and truth-matched signal distributions from MC are consistent. (d) Systematic effects from the χ_{vtx}^2 requirement are considered, since the signal and reference modes have different χ_{vtx}^2 distributions. We change the requirement to $\chi_{\text{vtx}}^2 < 21$ and repeat our measurement. The resulting changes to the nominal results, 0.6% and 0.3%, are small as expected and assigned as the corresponding systematic uncertainties. (e) The uncertainty due to the π^0 veto for η candidates in $\Lambda_c^+ \rightarrow pK_S^0 \eta$ is estimated by enlarging the veto region from ± 12.5 MeV/ c^2 to be ± 15 MeV/ c^2 . The resulting change on the branching fraction is 0.2%, and is assigned as a systematic uncertainty. (f) The uncertainty due to limited MC statistics for efficiency value is 0.1%.

The uncertainty due to the non- K_S^0 peaking background is estimated based on the generic MC sample aforementioned. As the rate of this background may depend on intermediate processes, we double its size, and take the resulting ratio with the signal yield, 0.8%, as the associated systematic uncertainty. The uncertainties on $\mathcal{B}(K_S^0 \rightarrow \pi^+ \pi^-) = (69.20 \pm 0.05)\%$ ($\delta\mathcal{B}/\mathcal{B} = 0.1\%$) and $\mathcal{B}(\eta \rightarrow \gamma\gamma) = (39.41 \pm 0.20)\%$ ($\delta\mathcal{B}/\mathcal{B} = 0.5\%$) are also considered. All uncertainties above are added in quadrature to give an overall systematic uncertainty, as listed in Table II. Additionally, the uncertainty from the world average branching fraction of the reference mode (5.0%) is considered.

VII. SUMMARY

In summary, based on the entire dataset with an integrated luminosity of 980 fb^{-1} collected by the Belle detector at the KEKB energy-asymmetric e^+e^- collider, we present the first observation of SCS decay $\Lambda_c^+ \rightarrow pK_S^0 K_S^0$ with a large statistical significance of $>10\sigma$, and measure the branching fractions of $\Lambda_c^+ \rightarrow pK_S^0 K_S^0$ and $\Lambda_c^+ \rightarrow pK_S^0 \eta$ relative to $\Lambda_c^+ \rightarrow pK_S^0$:

$$\frac{\mathcal{B}(\Lambda_c^+ \rightarrow pK_S^0 K_S^0)}{\mathcal{B}(\Lambda_c^+ \rightarrow pK_S^0)} = (1.47 \pm 0.08 \pm 0.04) \times 10^{-2}, \quad (10)$$

$$\frac{\mathcal{B}(\Lambda_c^+ \rightarrow pK_S^0 \eta)}{\mathcal{B}(\Lambda_c^+ \rightarrow pK_S^0)} = (2.72 \pm 0.06 \pm 0.13) \times 10^{-1}, \quad (11)$$

where the uncertainties are statistical and systematic, respectively, Using the world average $\mathcal{B}(\Lambda_c^+ \rightarrow pK_S^0) = (1.59 \pm 0.08)\%$ [17], we obtain the absolute branching fractions

$$\mathcal{B}(\Lambda_c^+ \rightarrow pK_S^0 K_S^0) = (2.34 \pm 0.12 \pm 0.06 \pm 0.12) \times 10^{-4}, \quad (12)$$

$$\mathcal{B}(\Lambda_c^+ \rightarrow pK_S^0 \eta) = (4.32 \pm 0.10 \pm 0.20 \pm 0.22) \times 10^{-3}, \quad (13)$$

where the first uncertainties are statistical, the second systematic, and the third from the uncertainty on $\mathcal{B}(\Lambda_c^+ \rightarrow pK_S^0)$. The first of these branching fractions is measured for the first time and found to be much smaller than the theoretical prediction of $(1.9 \pm 0.4) \times 10^{-3}$ [19]. The latter one is consistent with the world average, $(4.15 \pm 0.90) \times 10^{-3}$ [17], and has a precision improved by threefold.

We also show the Dalitz plots of $\Lambda_c^+ \rightarrow pK_S^0 K_S^0$ and $\Lambda_c^+ \rightarrow pK_S^0 \eta$ after background subtraction and efficiency correction, and find two clear structures: $f_0(980)$ or $a_0(980)$ decaying into $K_S^0 K_S^0$ and $N^*(1535)$ decaying into $p\eta$. This indicates that amplitude analyses of these decays, which will be possible using the large datasets that will become available at BESIII [42] or Belle II [43], may help understand the nature of such intermediate resonances.

ACKNOWLEDGMENTS

L. K. Li thanks Li-Sheng Geng and Ju-Jun Xie for helpful discussions on the $N^*(1535)$. We thank the KEKB group for the excellent operation of the accelerator, and the KEK cryogenics group for the efficient operation of the solenoid.

- [1] Q. P. Xu and A. N. Kamal, *Phys. Rev. D* **46**, 270 (1992).
- [2] H.-Y. Cheng and B. Tseng, *Phys. Rev. D* **48**, 4188 (1993).
- [3] J. G. Korner and M. Kramer, *Z. Phys. C* **55**, 659 (1992).
- [4] M. A. Ivanov, J. G. Korner, V. E. Lyubovitskij, and A. G. Rusetsky, *Phys. Rev. D* **57**, 5632 (1998).
- [5] K. K. Sharma and R. C. Verma, *Eur. Phys. J. C* **7**, 217 (1999).
- [6] J. Zou, F. Xu, G. Meng, and H.-Y. Cheng, *Phys. Rev. D* **101**, 014011 (2020).
- [7] H.-Y. Cheng, X.-W. Kang, and F. Xu, *Phys. Rev. D* **97**, 074028 (2018).
- [8] C.-D. Lü, W. Wang, and F.-S. Yu, *Phys. Rev. D* **93**, 056008 (2016).
- [9] C. Q. Geng, C.-W. Liu, and T.-H. Tsai, *Phys. Lett. B* **794**, 19 (2019).
- [10] C.-Q. Geng, C.-W. Liu, T.-H. Tsai, and Y. Yu, *Phys. Rev. D* **99**, 114022 (2019).
- [11] J. Brod, A. L. Kagan, and J. Zupan, *Phys. Rev. D* **86**, 014023 (2012).
- [12] H.-Y. Cheng and C.-W. Chiang, *Phys. Rev. D* **85**, 034036 (2012).
- [13] H.-n. Li, C.-D. Lu, and F.-S. Yu, *Phys. Rev. D* **86**, 036012 (2012).
- [14] Y. Grossman, A. L. Kagan, and Y. Nir, *Phys. Rev. D* **75**, 036008 (2007).
- [15] Y. Grossman, A. L. Kagan, and J. Zupan, *Phys. Rev. D* **85**, 114036 (2012).
- [16] W. Altmannshofer, R. Primulando, C.-T. Yu, and F. Yu, *JHEP* **04**, 049 (2012).
- [17] R. L. Workman *et al.* (Particle Data Group), *Prog. Theor. Exp. Phys.* **2022**, 083C01 (2022).
- [18] Throughout this paper, the charge-conjugate modes are implied.
- [19] J.-Y. Cen, C.-Q. Geng, C.-W. Liu, and T.-H. Tsai, *Eur. Phys. J. C* **79**, 946 (2019).
- [20] S. Capstick and W. Roberts, *Prog. Part. Nucl. Phys.* **45**, S241 (2000).
- [21] J.-J. Xie and L.-S. Geng, *Phys. Rev. D* **96**, 054009 (2017).
- [22] R. Pavao, S. Sakai, and E. Oset, *Phys. Rev. C* **98**, 015201 (2018).
- [23] B.-S. Zou, *Nucl. Phys. A* **835**, 199 (2010).
- [24] F.-K. Guo, C. Hanhart, U.-G. Meißner, Q. Wang, Q. Zhao, and B.-S. Zou, *Rev. Mod. Phys.* **90**, 015004 (2018).
- [25] N. N. Achasov, J. V. Bennett, A. V. Kiselev, E. A. Kozyrev, and G. N. Shestakov, *Phys. Rev. D* **103**, 014010 (2021).
- [26] Z.-Q. Wang, X.-W. Kang, J. A. Oller, and L. Zhang, *Phys. Rev. D* **105**, 074016 (2022).
- [27] M. G. Alford and R. L. Jaffe, *Nucl. Phys. B* **578**, 367 (2000).
- [28] L. Maiani, F. Piccinini, A. D. Polosa, and V. Riquer, *Phys. Rev. Lett.* **93**, 212002 (2004).
- [29] G. 't Hooft, G. Isidori, L. Maiani, A. D. Polosa, and V. Riquer, *Phys. Lett. B* **662**, 424 (2008).
- [30] J. D. Weinstein and N. Isgur, *Phys. Rev. D* **41**, 2236 (1990).
- [31] V. Baru, J. Haidenbauer, C. Hanhart, Y. Kalashnikova, and A. E. Kudryavtsev, *Phys. Lett. B* **586**, 53 (2004).
- [32] A. Abashian *et al.* (Belle Collaboration), *Nucl. Instrum. Meth. A* **479**, 117 (2002); also see Section 2 in J. Brodz-

- icka *et al.*, *Prog. Theor. Exp. Phys.* **2012**, 04D001 (2012).
- [33] S. Kurokawa and E. Kikutani, *Nucl. Instrum. Meth. A* **499**, 1 (2003), and other papers included in this Volume; T. Abe *et al.*, *Prog. Theor. Exp. Phys.* **2013**, 03A001 (2013) and references therein.
- [34] D. J. Lange, *Nucl. Instrum. Meth. A* **462**, 152 (2001).
- [35] T. Sjöstrand, P. Edén, C. Friberg, L. Lönnblad, G. Miu, S. Mrenna, and E. Norrbin, *Comput. Phys. Commun.* **135**, 238 (2001).
- [36] R. Brun *et al.*, CERN Report No. CERN-DD-EE-84-1 (1987).
- [37] E. Barberio and Z. Was, *Comput. Phys. Commun.* **79**, 291 (1994).
- [38] E. Nakano, *Nucl. Instrum. Meth. A* **494**, 402 (2002).
- [39] M. Feindt and U. Kerzel, *Nucl. Instrum. Meth. A* **559**, 190 (2006).
- [40] H. Nakano, Ph.D Thesis, Tohoku University (2014), Chapter 4, <http://hdl.handle.net/10097/58814>.
- [41] M. Pivk and F. R. Le Diberder, *Nucl. Instrum. Meth. A* **555**, 356 (2005).
- [42] M. Ablikim *et al.* (BESIII Collaboration), *Chin. Phys. C* **44**, 040001 (2020).
- [43] E. Kou *et al.*, *Prog. Theor. Exp. Phys.* **2019**, 123C01 (2019).